

Energy Conservation Model for Electromechanical Transient Characteristics of Electromagnetic Actuators

Jiaxin You, *Member, IEEE*, Rao Fu, Huimin Liang, *Member, IEEE*,
Dazhi Yang, Yigang Lin, and Venkata Dinavahi, *Fellow, IEEE*

Abstract—Fault diagnosis and bounce reduction of electromagnetic actuators require one to obtain the electromechanical transient characteristics (ETCs) in real-time. ETCs can be measured by sensors, but due to their large size and intrusiveness, the approach has its limitations. Acquiring ETCs through finite element method (FEM) could be an alternative, except that FEM is known to be time consuming. In contrast, real-time measurement of coil current is not subjected to these restrictions, yet, it has not been properly utilized for calculating ETCs. In this regard, this paper analyzes the source of the armature kinetic energy, and thus proposes a model based on energy conservation (ECM), describing the relationship between the mechanical and electrical characteristics. Based on the model, ETCs can be calculated from coil current, moving part mass, and the static counterforce. To exemplify the effectiveness of the procedure, an electromagnetic contactor is considered, and the results obtained using the ECM are found fairly consistent with that obtained using sensors. The merit of the proposed ECM lies in its non-intrusive nature and its ability to circumvent the time-consuming FEM in calculating ETCs.

Index Terms—Bounce reduction, coil current, electromagnetic actuators, energy conservation, fault diagnosis, real-time systems, sensors, transient characteristics.

I. INTRODUCTION

ELECTROMAGNETIC actuators are widely used as industrial devices such as relays, contactors, circuit breakers, or solenoid valves. However, as the reliability of electromagnetic actuators has hitherto been a concern, which may greatly limit their lifespan, manufacturers today offer devices that come with electronic control units, as an effort to reduce problems (such as arcing) associated with contact bounce. Various feedback control techniques have been proposed [1], [2], which are able to limit the coil power supply to reduce the collision kinetic energy of the contact, and thereby reduce bounce. Besides bounce reduction, real-time fault diagnosis, which seeks to continuously monitor the health of the device, is also seen as a vital measure to improve reliability [3]–[5]. Insofar as reliability and lifespan are concerned, it is known *a priori* that the pick-up time, release time, and shock resistance of an actuator are relevant properties. These properties are related to the electromechanical transient characteristics (ETCs) of the actuator, which refer to the speed and displacement of the armature, the electromagnetic force, and the counterforce in transient process [6]. In that, obtaining the real-time ETCs constitutes a preceding step in bounce reduction and fault diagnosis of electromagnetic actuators.

Real-time ETCs can be directly measured using sensors. For instance, Liu *et al.* [7] used an acceleration sensor to measure the displacement of the circuit breaker, in order to study the dynamic resistance. On another occasion, a displacement sensor was employed to acquire the displacement data of the contact [8], as a means to estimate the remaining service life of the breakers. Nevertheless, the installation of displacement sensors requires a certain amount of space (see Fig. 1), which limits their uptake [9]. Additionally, the sealed case has to be opened, such that the sensor's laser can gain a field-of-view on the subject that is being measured. Though it is an efficient and accurate method for obtaining ETCs, sensors are bulky and intrusive, which often place constraints on the size of the subject and the application environment.

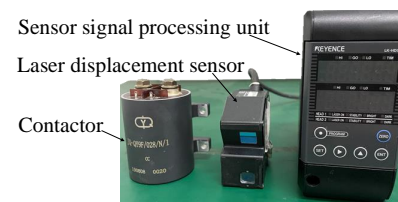


Fig. 1. An example showing the size of a displacement sensor relative to a contactor and a sensor signal processing unit.

Due to the aforementioned limitations of sensors, finite element method (FEM), which is a computerized method for predicting how a product reacts to real-world physical forces, has been widely used as an alternative for obtaining ETCs. FEM not only reduces the effort that is required for trial-and-error on experiment design, setup, and optimization, but also is able to observe more detailed data. FEM has been used to calculate the nonlinear relationship among displacement, flux linkage, and current [10]–[13], and to calculate the displacement and coil current under various fault conditions [14]. In principle, FEM-based ETCs estimation needs to solve a set of differential equations based on Maxwell's equations. Basically, that is a complex, difficult, and time-consuming procedure [15]. To reduce the computational time of FEM, fully coupled simulation framework [16], re-meshing technique [17], fast algorithm [18] and the equivalent circuit method of the coil-coil type electromagnetic repulsion actuator [19] have been developed successively. These efforts were found to be able to reduce the computational time of FEM to some extent; at any rate, that is still far from real-time applications.

In order to be free from space constraints and to meet the requirements for real-time calculation, a third class of methods of acquiring ETCs is to infer it from coil current, of which the measurement is much simpler than measuring ETCs themselves. Methods of this sort include mainly the sliding-mode observer (SMO) method and inference through coil inductance. A nonlinear SMO was designed to observe the spool position, which has led to significant reduction of noise and braking of the paddle vibration [20] while achieving soft landing of the solenoid valve [21], [22]. Notwithstanding, owing to its complex and intricate computations, the computational stability of SMO is often limited. On the other hand, some have suggested inferring ETCs via calculating the coil inductance from the coil current, in that, its the computational stability is not limited. Rahman *et al.* [23] drew the boundary on the position inductance table to ensure the accuracy of the position estimation. The coil inductance varies with displacement and current, which are related to electromagnetic force [24], [25]. More generally, the relationship between inductance and ETCs is the problem that needs to be addressed. Ramirez-Laboreo and colleagues have contributed much in this regard; their works include the estimation of coil inductance based on gap [26], [27] or coil current [28], and magnetic flux model considering eddy current, hysteresis and saturation [29]. These works have shown that it is possible to estimate ETCs without sensors, but based on the coil inductance. To further improve the accuracy of estimation, and to calculate the armature displacement in real-time, the relationship models between the armature displacement and the coil inductance, the coil turns, and the magnetic circuit cross-section, were established. These parameters were used as the input of the the bounce reduction algorithm [1], [2], [26], [30]. Notwithstanding, when the circuit breaker operates under high current, the aerodynamic repulsion force reduces the movement speed of the armature and changes the armature displacement. These effects are not reflected in the above-mentioned simplified models of coil inductance, since they ignore the influence of the armature speed on the coil inductance.

To address the limitations of the intricate computations of SMO and the negligence of armature speed in simplified models of coil inductance, it is necessary to develop a general real-time method for ETCs computation based on the coil current. A model based on energy conservation (ECM) is herein proposed to establish the relationship between the mechanical characteristics (electromechanical transient characteristics) and the electrical characteristics (coil current). The main contributions are as follows:

- 1) Only the coil current, the mass of moving parts, and the counterforce are required (see in Section II-A Eq. (10)). The model takes into account the interaction between the speed and displacement of the armature, and the coil current. In this regard, the ECM provides a more realistic way to calculate ETCs in real-time as compared to the simplified models.
- 2) The ECM is proposed to establish the relationship between the mechanical characteristics and the electrical characteristics. Besides, it uses the coil current to cal-

culate electromagnetic force, thereby circumventing the needs for solving the complex Maxwell's equations with the FEM framework or SMO.

The remaining part of the paper is organized as follows. Section II discusses the theory of the ECM, and Section III describes its application. Section IV discusses the results and compares the scope of existing methods. Section V presents the conclusion and potential future extensions.

II. THEORY OF THE ECM

This section introduces the ECM in part A and key node of the ECM in part B, and analyze coil inductance transients in part C.

A. The ECM of the ETCs

The mathematical representation of a coil loaded with voltage can be expressed as follows:

$$u = r \cdot i(t) + \frac{d\psi(t)}{dt}, \quad (1)$$

$$\psi(t) = l(t) \cdot i(t), \quad (2)$$

where u is the power supply voltage, r is the coil resistance, $i(t)$ is coil current, $l(t)$ is coil inductance, and $\psi(t)$ is the flux linkage of the electromagnetic system. Both u and r are assumed to be constant.

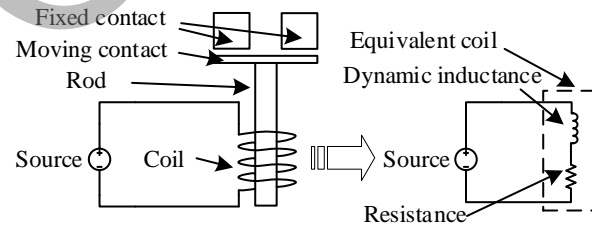


Fig. 2. Equivalent circuit of coil circuit.

The equivalent circuit of the coil, which consists of a resistor and an inductor in series, is shown in Fig. 2. Once the coil is energized, the electrical energy is converted into heat through the resistance and magnetic energy through the coil. According to the law of energy conservation, such energy balance is expressed as follows:

$$w_{\text{power}} = w_{\text{res}} + w_{\text{mag}}, \quad (3)$$

$$w_{\text{power}} = \int u \cdot i(t) dt, \quad (4)$$

$$w_{\text{res}} = \int r \cdot i^2(t) dt, \quad (5)$$

where w_{power} is the energy provided by the power supply, w_{res} is the power consumption of the resistor, and w_{mag} is the magnetic energy required to establish the magnetic field.

Concerning w_{mag} during the energy conversion, part of the initial energy is stored in the coil, and the other portion would be converted into mechanical (kinetic) energy, which leads to the armature movement, i.e.,

$$w_{\text{mag}} = w_{\text{coil}} + w_{\text{mech}}, \quad (6)$$

where w_{coil} is the energy stored in the coil, w_{mech} is the kinetic energy of the armature. It is then apparent that, in order to calculate the kinetic energy of the armature movement, the stored energy in the coil inductance must be known.

On the one hand, combining Eqs. (3)–(6), one yields:

$$\begin{aligned} w_{\text{mech}} &= w_{\text{mag}} - w_{\text{coil}} \\ &= \int (u - r \cdot i(t)) \cdot i(t) dt - w_{\text{coil}}. \end{aligned} \quad (7)$$

On the other hand, the kinetic energy of the armature is the combined result of an electromagnetic force and a counterforce provided by springs, of which the relationship can be expressed as:

$$\frac{1}{2}mv^2 = w_{\text{mech}} - (F_{\text{coun}} + mg)\Delta S, \quad (8)$$

where m and v are the mass and speed of the moving part, respectively, F_{coun} is the counterforce provided by the spring, ΔS is the displacement of the moving part in a time interval, and g is gravitational acceleration. It follows from Eqs. (7) and (8) that:

$$\begin{aligned} w_{\text{mech}} &= \frac{1}{2}mv^2 + (F_{\text{coun}} + mg)\Delta S \\ &= \int (u - r \cdot i(t)) \cdot i(t) dt - w_{\text{coil}}. \end{aligned} \quad (9)$$

Finally, differentiating Eq. (9) with respect to t results in the ECM of transient characteristics:

$$mv \frac{dv}{dt} + (F_{\text{coun}} + mg)v = u \cdot i(t) - \left[r \cdot i^2(t) + \frac{dw_{\text{coil}}}{dt} \right]. \quad (10)$$

w_{coil} is calculated through Eq. (12) based on an discretization of the armature speed, of which the details are to be elaborated in Section II-B, and u , $i(t)$ and r can be calculated based on Section III-A1, m , F_{coun} , can be measured in Section III-A2. S , v and the transient force calculated by v are the ETCs.

B. Assumption of the coil energy

Different from the air-core coil, the inductance of a coil with armature is nonlinear with respect to time, and how to obtain the energy w_{coil} absorbed by the coil inductance, see Eq. (10), is the primary problem of concern for the proposed ECM. In Fig. 2, the voltage of the coil inductance is $u - r \cdot i(t)$ and the current flowing in is $i(t)$. Energy absorbed by a coil with armature is expressed as follows:

$$\begin{aligned} w_{\text{coil}} &= \int P_{\text{coil}} dt \\ &= \int (u - r \cdot i(t)) \cdot i(t) dt \\ &= w_{\text{mag}}, \end{aligned} \quad (11)$$

where P_{coil} is the power stored in the coil. By substituting Eq. (11) into Eq. (7), one has $w_{\text{mech}} = 0$, which implies that the armature is at rest. If the armature is in motion, it must occupies a part of the coil voltage, which implies that Eq. (11) is unsuitable to describe the current system. Consequently, assumption about the coil with armature need to be made, and the expression for w_{coil} needs to be modified.

About the coil with armature, which is expressed as nonlinear inductance with respect to time, this paper considers the following assumption. An inductance that is nonlinear with respect to time can be divided into infinitesimal time intervals. In each time interval, the inductance is a fixed value, as shown in Fig. 3. And the voltage of the coil inductance is $l(t) \cdot \frac{di(t)}{dt}$ in a time interval and the current flowing in is $i(t)$. This paper argues the discretization allows the coil energy in a time interval to be expressed as:

$$\begin{aligned} w_{\text{coil}} &= \int P_{\text{coil}} dt \\ &= \int l(t) \cdot \frac{di(t)}{dt} \cdot i(t) dt \\ &= l(t) \int i(t) di(t) \\ &= \frac{1}{2}l(t) \cdot i^2(t), \end{aligned} \quad (12)$$

$l(t)$ is the inductance of the coil, which is time-varying throughout the transient, but fixed in each time interval.

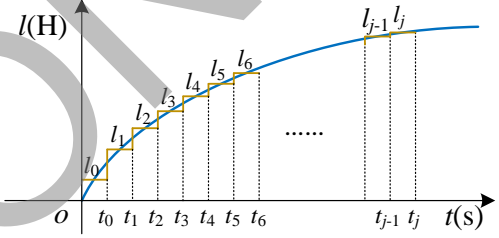


Fig. 3. Discretization of the inductance of a coil with armature.

When Eq. (12) is used with Eq. (6), the obtained w_{mech} includes the energy of the armature movement and the iron loss. It should be noted that, in this article, we only discuss electromagnetic parts, which consist of a coil, an iron core, an armature, and a yoke iron, with high linearity, i.e. iron losses can be ignored. Therefore, w_{mech} is just the kinetic energy of the armature.

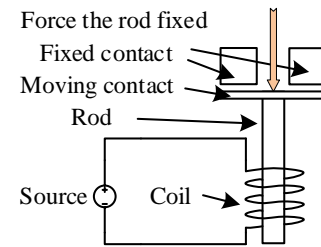


Fig. 4. Fixed armature setup.

Generally, a coil with armature is considered as nonlinear inductance with respect to time. Even if the armature is fixed, its inductance is time-varying. If the above assumption about the coil with armature is reasonable to describe the movement of the armature, Eq. (12) should also hold for the case of the fixed armature. And then, it should be deduced that w_{mech} mentioned by Eq. (6) is always equal to zero in the transient, i.e., the power P_{coil} (shown in Eq. (13)) stored in the coil

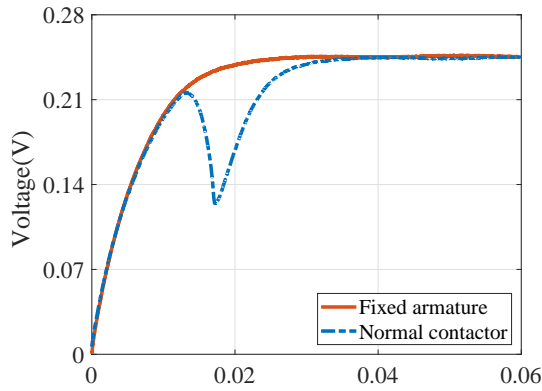


Fig. 5. Coil current (sampling voltage of u_2 in Fig. 11) of fixed armature and normal contactor.

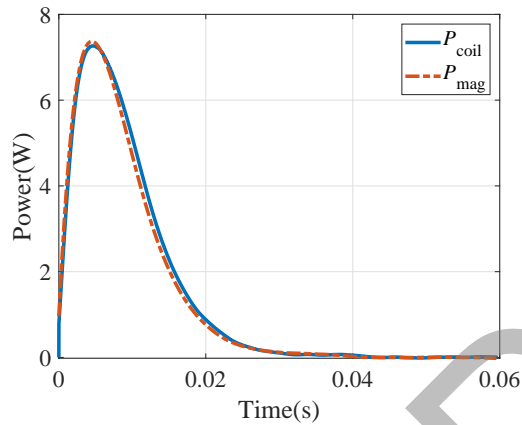


Fig. 6. Power of coil inductance and magnetic field.

inductance is equal to the power P_{mag} (shown in Eq. (14)) consumed to establish the magnetic field, which is consistent with the fact that the armature does not move in the case of the fixed armature.

$$P_{\text{coil}} = dw_{\text{coil}}/dt, \quad (13)$$

$$P_{\text{mag}} = dw_{\text{mag}}/dt. \quad (14)$$

To perform a quick sanity check on the assumption, the coil current with a fixed armature (see in Fig. 4) is sampled and compared with that of a normal contactor. Figure 5 depicts these two transients. P_{coil} and P_{mag} show high correspondence (see in Fig. 6), and hence suggests that w_{mech} is close to zero, confirming the validity of the assumption.

C. Analysis of coil inductance during the armature movement

Before we proceed to the detailed calculation, changes in the coil inductance during the armature movement should be analyzed. As shown in Fig. 7, comparing the transient of coil current of the fixed armature and normal contactor, the energy consumption, as enclosed by $b-c-d-e-f-b$, is due to the motion of the armature.

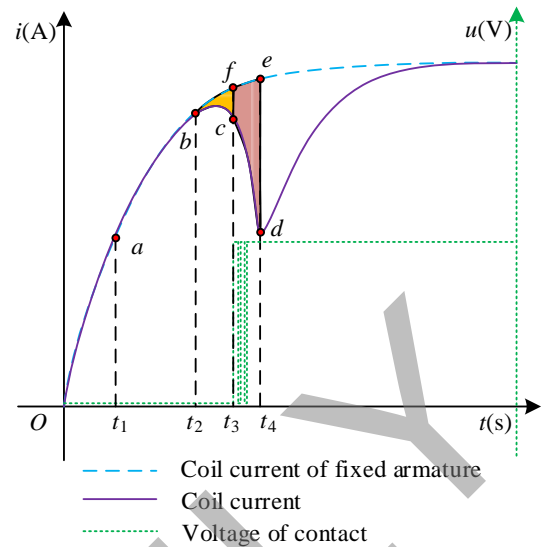


Fig. 7. Coil current and contact potential of the contactor.

When the coil with armature is loaded with current, the inductance is expressed according Eqs. (1) and (2) as follows:

$$l_1(t) = \frac{d\psi(t)/dt}{di(t)/dt} = \frac{u - r \cdot i(t)}{di(t)/dt}, \quad (15)$$

$$l_2(t) = \frac{\psi(t)}{i(t)} = \frac{\int u - r \cdot i(t) dt}{i(t)}. \quad (16)$$

When the inductance fluctuates around a fixed value, Eq. (15) holds. In the other case, Eq. (16) holds. It needs to be explained here why Eq. (16) does not apply when the inductance fluctuates around a fixed value. Differentiate $\psi(t)$ as follows:

$$\frac{d\psi(t)}{dt} = l(t) \cdot \frac{di(t)}{dt} + i(t) \cdot \frac{dl(t)}{dt}, \quad (17)$$

$$\frac{dl(t)}{dt} \approx 0. \quad (18)$$

At fixed value stage, due to iron loss, the inductance fluctuates around a fixed value, Eq. (18) holds. If Eq. (16) were applied in fixed value stage, the interference from eddy current, etc. would be magnified and included in the inductance by its integral arithmetic. In any case, Eq. (15) is more appropriate than Eq. (16).

During the interval $0-t_1$, the coil current exhibits fast growth. Due to the hysteresis effect, weak changes in magnetic induction provide negligible electromagnetic force. The inductance is a fixed value, and Eq. (15) applies for this period. At t_1 , the electromagnetic system begins to provide electromagnetic force, but such force is not sufficient to move the armature, the displacement and speed of the armature are therefore zero, and the magnetoresistance, which affects the inductance more than the electromagnetic force, has not changed. Besides, a portion of the energy that should be used to create the magnetic field is taken up, and the inductance is reduced to accommodate this change. Fixed value inductance changes into a variable linear inductance and Eq. (16) applies in this period.

During the interval t_1-t_2 , the electromagnetic force provided by the electromagnetic system is less than the counterforce

of provided by the counterforce spring at the initial position of the armature. The armature does not move, and the inductance gradually decreases. At t_2 , the electromagnetic force provided by the system is equal to the counterforce of the armature at initial position. At this precise moment, changes in the displacement and speed of the armature occur, resulting in a change in magneto-resistance, the change in inductance introduced by the electromagnetic force is hedged out, and the inductance stops decreasing and begins increasing.

During the interval t_2-t_3 , the electromagnetic force provided by the system is larger than the counterforce (only counterforce spring provides) of the armature. As the armature moves, its displacement and magneto-resistance increase gradually and the inductance increases gradually. At t_3 , the armature begins the over-travel, the inductance continues to increase.

During the interval t_3-t_4 , the counterforce (as provided by both the over-travel spring and counterforce spring) on the armature increases further, the displacement of the armature enters the over travel range, and the inductance continues to increase. At t_4 , the displacement of the armature reaches its maximum. As the armature bounces, the magneto-resistance and inductance saturates to a fixed value. To visualize the above-mentioned operating process, the electromagnetic force, counterforce and inductance, as functions of time, are shown in Fig. 8.

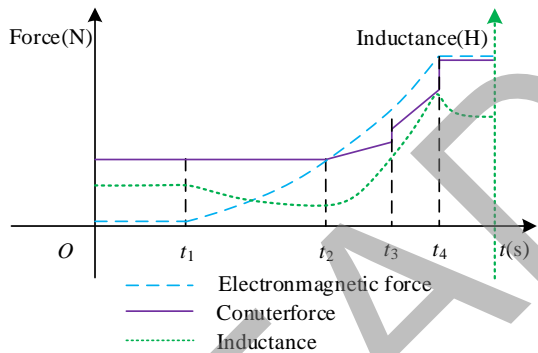


Fig. 8. Electromagnetic force, counterforce and inductance in the movement.

III. APPLICATION OF THE ECM

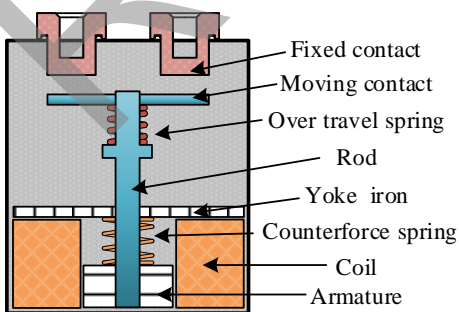


Fig. 9. Internal structure of the contactor.

The empirical part of the paper considers a 270V/200A contactor. The cross-sectional view of the contactor is shown

in Fig. 9. As electric current flows through the coil of the contactor, it generates the electromagnetic force that moves the armature. This is achieved by switching on and off the contact that control the main circuit. Various components in the contactor can be divided into an electromagnetic part and a contact part. The electromagnetic part provides electromagnetic force when the coil is loaded with voltage. It consists of a coil, an iron core, an armature, and a yoke iron. The contact part provides the counterforce, and it consists of moving contacts, fixed contacts, and springs.

A. Required data

If we are to calculate ETCs the coil current from Eq. (10), the mass of the moving parts and the counterforce are required. Therefore, this section describes the procedure of measuring these quantities.

1) *Measuring power supply voltage, coil current and coil resistance:* Using an oscilloscope, sensor resistor, power, and switch, the coil current sampling circuit is built, as shown in Fig. 10. The contactor is equivalent to a combination of inductance, resistance, and a switch. The equivalent circuit of the contactor is depicted in Fig. 11. u_1 can be obtained directly from the supply voltage, which corresponds to u in Eq. (10). The oscilloscope triggers the sampling to obtain the potentials u_2 and u_3 . The value of r_2 is known, and the coil current $i(t)$ is obtained by dividing u_2 with r_2 :

$$i(t) = \frac{u_2(t)}{r_2}. \quad (19)$$

The oscilloscope samples the potentials u_2 and u_3 , and the results are shown in Fig. 12. u_3 can be used to characterize the opening, closing, bounce, over travel starting point of the contactor. The formula for obtaining r_1 is shown in Eq. (20), which corresponds to r in Eq. (10). u_2' is the steady state value of u_2 , and when t is greater than 0.05 s (see in Fig. 12), u_2 remains stable:

$$r_1 = \frac{u_1}{u_2'/r_2} - r_2. \quad (20)$$

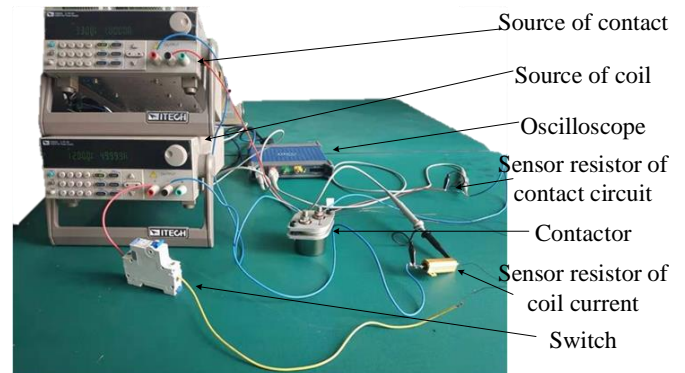


Fig. 10. Coil current sampling circuit experiment.

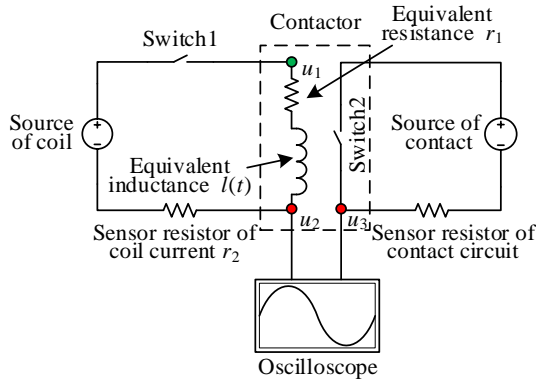


Fig. 11. Coil current sampling equivalent circuit.

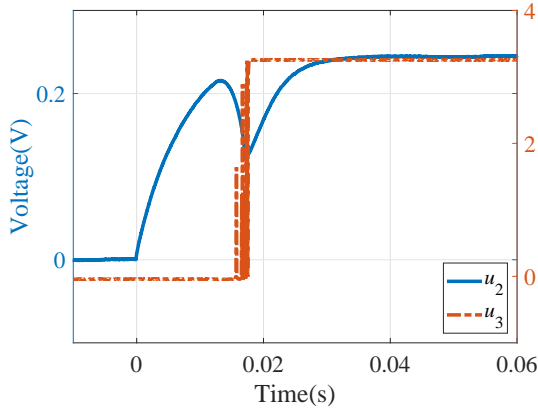


Fig. 12. Coil current u_2 , contact potential u_3 .

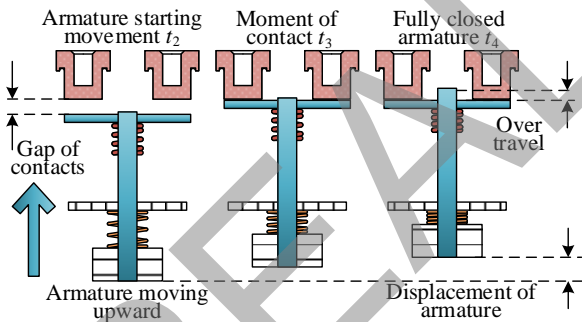


Fig. 13. Process of armature movement.

2) *Measuring the counterforce and the mass of moving parts:* In our device, the counterforce is provided by two springs. The operation of the armature is shown in Fig. 13. The process is divided into two stages.

- 1) From the moment when the armature starts moving (i.e., t_2) to the moment of contacting (i.e., t_3), only the counterforce spring provides counterforce. The moving parts include contacts, counterforce spring, over travel spring, armature and iron core. The over-travel spring is also in the initial compression state, but it does not provide force.
- 2) From the moment of contacting (t_3) to a fully closed armature (t_4), over-travel spring and the counterforce

spring provide the counterforce jointly. At this instance, contacts no longer move, and thus the overall mass of the moving parts decrease. The moving parts include counterforce spring, over-travel spring, armature, and iron core, except contacts.

The time-varying curves of counterforce at t_2-t_4 is shown in Fig. 8. Measure the stiffness coefficient and the initial compression force of counter spring and over-travel spring to obtain the counterforce as follows:

$$F_{\text{coun}} = k_{\text{spring}}S + F_{\text{initial}}, \quad (21)$$

$$F_{\text{initial}} = \begin{cases} 5.36, & 0 < S < S_0 \\ -13431.20S_0 + 8.99, & S_0 \leq S \end{cases} \text{ N.} \quad (22)$$

where k_{spring} is the stiffness coefficient of the spring, measured as:

$$k_{\text{spring}} = \begin{cases} 759.96, & 0 < S < S_0 \\ 14191.16, & S_0 \leq S \end{cases} \text{ N/m,} \quad (23)$$

F_{initial} is the initial compression force of the spring, S is the displacement of the armature, and S_0 is the contact gap. Results show that the mass of the moving parts including the contacts is 22.69×10^{-3} kg, and the mass of the moving parts without the contacts is 15.15×10^{-3} kg as given by:

$$m = \begin{cases} 22.69 \times 10^{-3}, & 0 < S < S_0 \\ 15.15 \times 10^{-3}, & S_0 \leq S \end{cases} \text{ kg.} \quad (24)$$

B. Calculation flow

Flow chart for calculating the armature speed is shown in Fig. 14.

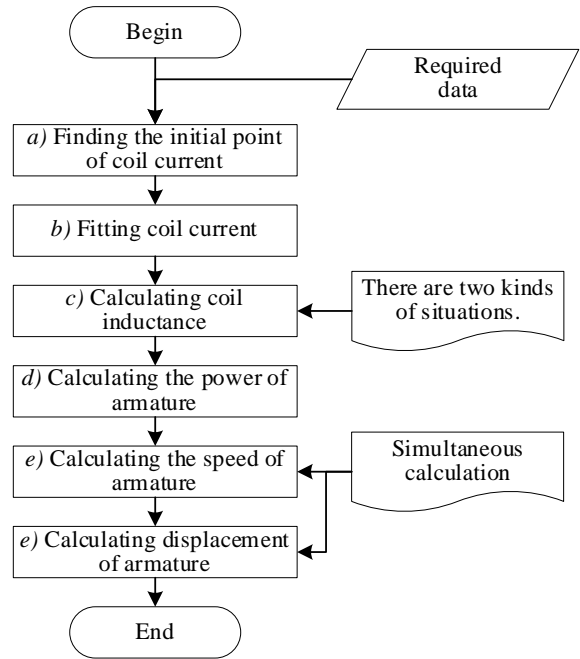


Fig. 14. Flow chart for calculating ETCs.

a) The initial value of u_2 acquired by the oscilloscope is not at the origin, and the initial point needs to be found.

b) From Eq. (10), it can be understood that the differential calculation is required. Since the noisy discrete data acquired

by the oscilloscope is not suitable for differential calculation, the data is smoothed and curve fitted, so that can be used for differential calculation.

c) The calculation of the coil inductance varies with its value, depending on whether it fluctuates around a fixed value or not. Due to the hysteresis effect, the inductance of the coil fluctuates about a fixed value for the interval $0-t_1$ after energization. After that, the inductance is a variable, so that there are two ways to calculate the inductance, as mentioned in second paragraph of Section II-C. At the interval $0-t_1$, it varies according to Eq. (15), and the calculation method is shown in Eq. (25). At the interval t_1-t_4 , it varies according to Eq. (16), and the calculation method is shown in Eq. (26):

$$l_1(t) = \frac{u_1 - u_2 - i_j r_1}{(i_j - i_{j-1}) / (t_j - t_{j-1})}, 0 < t < t_1, \quad (25)$$

$$l_2(t) = \frac{(u_1 - u_2 - i_j r_1)(t_j - t_{j-1}) + \psi_{j-1}}{i_j}, t_1 \leq t \leq t_4, \quad (26)$$

where t_j represents the current time, t_{j-1} is $t_j - \Delta t$, Δt is the time interval.

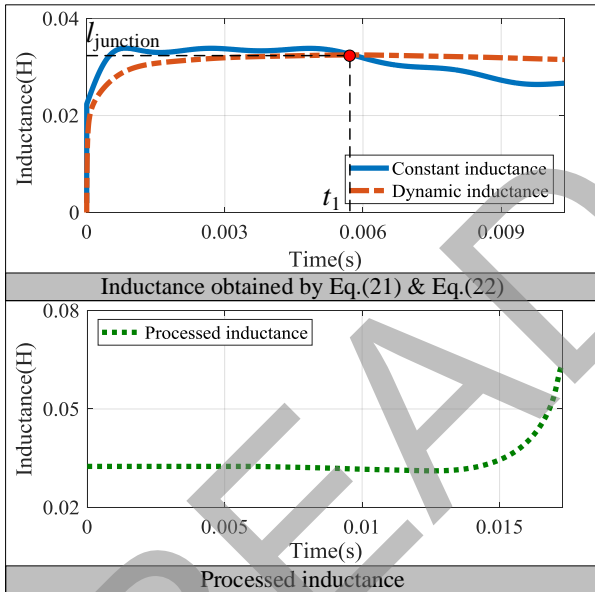


Fig. 15. Processed inductance of the coil.

The coil inductance is shown in Fig. 15. The inductance of the coil is approximately a fixed value for $t < t_1$, and after that the inductance starts to decrease. From Fig. 8, it can be observed that when t is less than t_1 , $l(t)$ is equal to l_{junction} as shown in Fig. 15. When t is greater than t_1 , $l(t)$ is equal to $l_2(t)$, as per Eq. (26).

d) The calculated armature power is shown in Fig. 16. When t is less than t_2 , the power of the armature fluctuates slightly about zero, due to the parasitic capacitance in the test loop and the iron losses, and does not cause any disturbance that is large enough to affect ETCs. Therefore, these fluctuations can be ignored and the power is zero if t is less than t_2 .

e) Due to the discrete nature data collected by the oscillo-

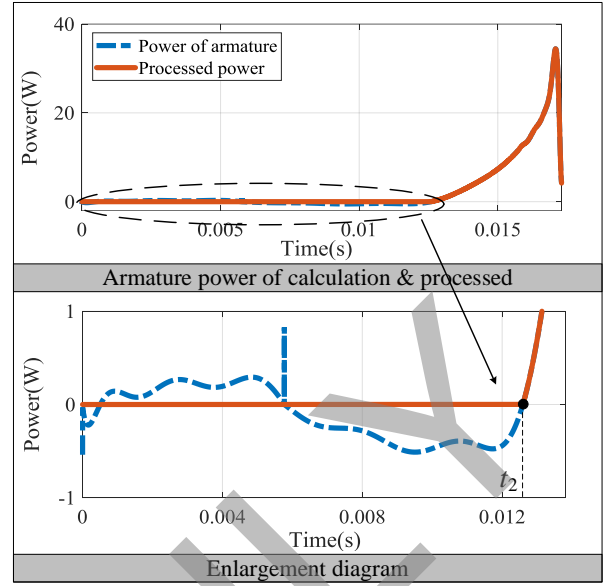


Fig. 16. Armature power in the transient process.

scope, Eq. (10) is discretized as:

$$mv_j \frac{v_j - v_{j-1}}{t_j - t_{j-1}} + \{k_{\text{spring}}[v_j(t_j - t_{j-1}) + S_{j-1}] + F_{\text{initial}} + mg\}v_j = u_1 i_j - \left(i_j^2 (r_1 + r_2) + \frac{1}{2} \frac{l_j i_j^2 - l_{j-1} i_{j-1}^2}{t_j - t_{j-1}} \right). \quad (27)$$

IV. RESULTS AND DISCUSSION

To validate the ECM, the results are compared with those obtained using the FEM- and sensor-based approaches. The test platform built for the verification the ECM is shown in Fig. 17. Whereas the coil current is measured using the oscilloscope, the armature displacement is measured by the laser displacement sensor. The speed and displacement of the armature are compared with the values obtained from FEM- and sensor-based approaches, see Fig. 18 and Fig. 19, respectively.

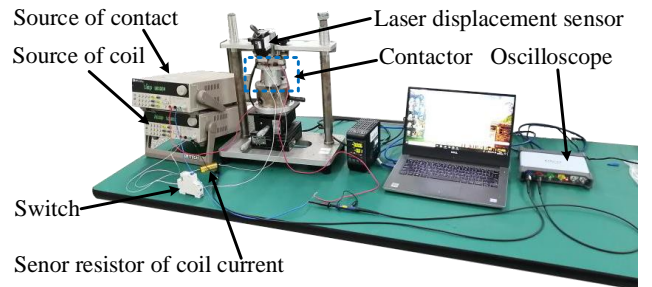


Fig. 17. Test platform for model verification.

In FEM, on the one hand, takes in known inputs include dimensions, the static counterforce and the magnetic properties of the material, and on the other hand, obtains the speed and displacement of the armature, the coil current, the transient electromagnetic force, the transient counterforce and

the contact pressure by solving Maxwell's equations. Here, the FEM can be regarded as three steps: (1) Altair Flux calculates the electromagnetic force under different current and armature displacement; (2) ADAMS (Automatic Dynamic Analysis of Mechanical Systems) sets the measured counterforce; (3) the continuous changes of armature speed and displacement under step voltage excitation are calculated by interpolation. The electromagnetic force obtained is steady-state data after the current and displacement are set by Altair Flux, without taking into account the interaction between the speed and displacement of the armature, and the coil current. The FEM is a forward process that requires additional consideration of complex interactions for more precise requirements, while ECM is a reverse process that does not need to calculate interactions because the coil current, which is the starting point of the calculation, contains information after complex interactions. Therefore, the FEM is not as accurate as ECM (see Fig. 18 and Fig. 19).

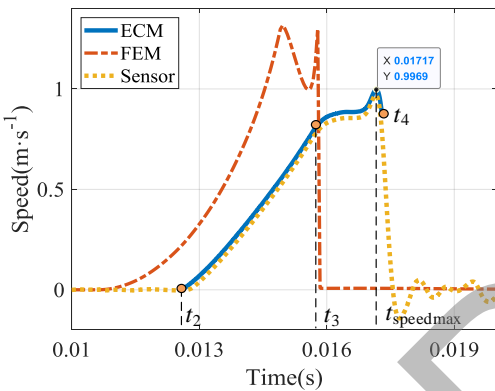


Fig. 18. Comparison of speed in ECM, FEM, and sensor.

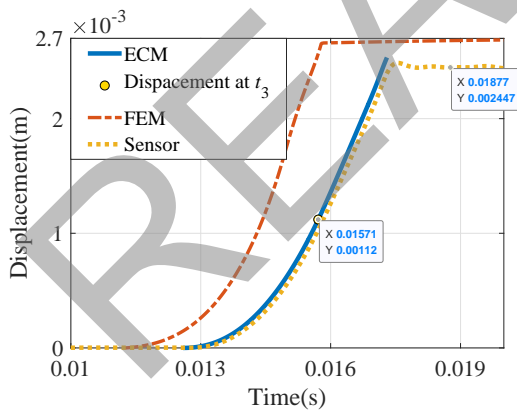


Fig. 19. Comparison of displacement in ECM, FEM, and sensor.

The ECM and measured armature displacements (and the speeds) clearly demonstrate an overall high correspondence, despite some differences at the armature's maximum displacement. This is owing to the fact that when the armature collides with the yoke iron, the counterforce suddenly increases and the armature bounces; this is, however, not accounted for by the ECM. The contact gap and the total armature displacement

of the sensor are 1.1 mm and 2.45 mm respectively, while these of the ECM are 1.12 mm and 2.53 mm respectively. Figure 20 shows the mechanical properties of the armature, which can be obtained by further calculating the speed and displacement of the armature. The electromagnetic force F_{mag} reaches the maximum value at 0.01706 s. When the resultant force is negative, the armature decelerates and continues to move forward until it reaches the maximum displacement. Finally, the armature collides with the yoke and bounces until it stabilizes.

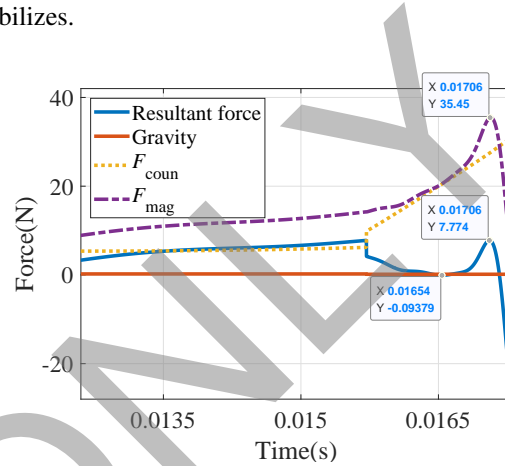


Fig. 20. Force in transient process of the contactor operation.

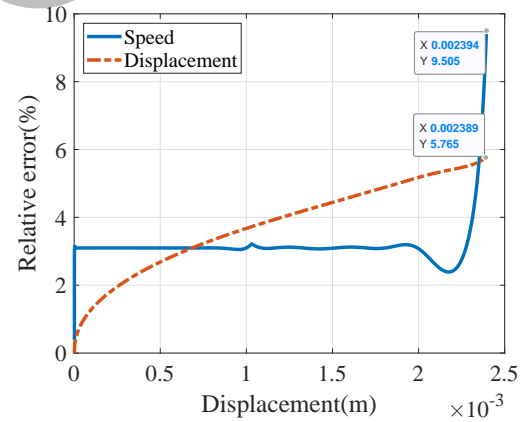


Fig. 21. Relative errors of speed and displacement.

Speed and displacement divided by the respective maximum value is shown in Fig. 21. When the armature approaches the end of over-travel, the relative error of speed increases sharply. This could be attributed to the increase of measurement error of the counterforce provided by the over-travel spring. The relative error of displacement increases gradually, and the increment is stable.

Errors of the ECM mainly comes from three aspects in descending order: (1) iron losses, (2) measurement errors of moving part mass, counterforce and current, and (3) time interval of the calculation. Relevant tests are carried out on 750V/630A contactor, comparisons of speed and displacement is shown in Fig. 22 and Fig. 23 respectively, and the relative errors are shown in Fig. 24. The relative error of speed rises

sharply, which is caused by the bounce at the end of the over-travel and exceeds the armature displacement considered by the ECM. At the end of the over-travel, the relative error of speed is 9.902%, which is less than 10% of maximum speed. Therefore, it is reasonable to believe that even for the high-voltage circuit breaker, the error should be less than 10% under the condition of low iron losses.

Due to the use of division instead of differentiation, the time interval of the calculation will also cause errors. According to the test data in Fig. 6, the analysis on time interval of the calculation is carried out as shown in Fig. 25. This error occurs only before the armature is closed. As the calculation interval decreases, the error reduces.

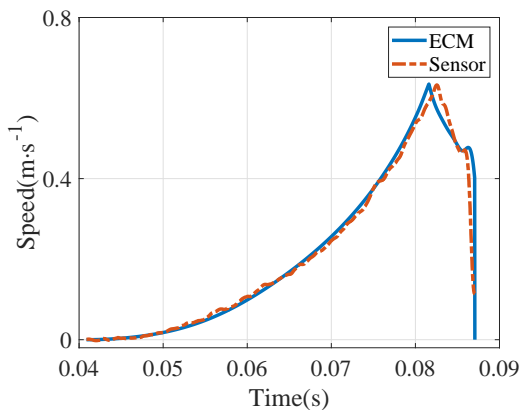


Fig. 22. Comparison of speed in ECM and sensor for 750V/630A contactors.

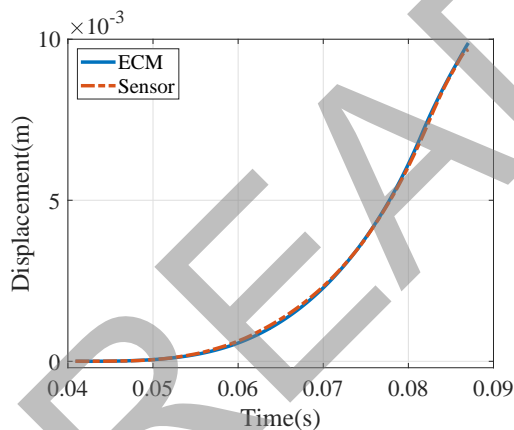


Fig. 23. Comparison of displacement in ECM and sensor for 750V/630A contactor.

The analysis made in this paper is based on the assumption described in Section II-B. Judging from the existing experimental results, the ECM is suitable for electromagnetic part with high linearity in which iron loss could be ignored. It is necessary to verify that it is suitable for situations with low linearity. The maximum error of two different target objects did not exceed 10% as shown in Fig. 21 and Fig. 24, it can be hypothesized that a relative error of more than 10% implies an electromagnetic part with significant low linearity, i.e. iron losses cannot be ignored, in which case the ECM cannot be applied.

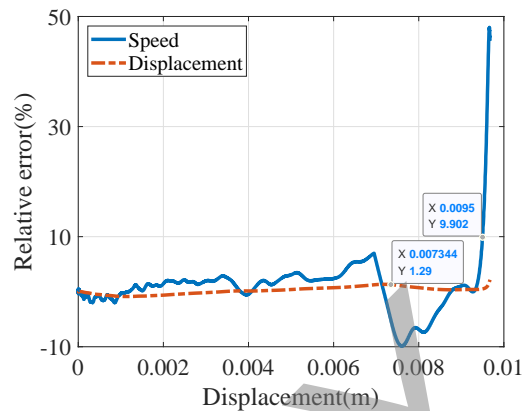


Fig. 24. Relative errors of speed and displacement for 750V/630A contactor.

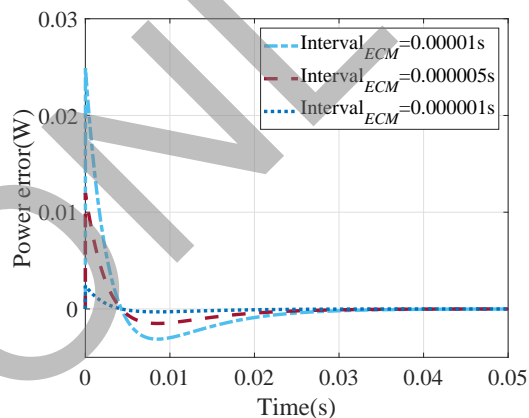


Fig. 25. Analysis on time interval.

Table I tabulates the differences among existing methods of a similar nature. Since the pros and cons are self-evident from the table, we do not elaborate too much on this account. In short, the proposed ECM can be used for fault diagnosis, design verification and the armature control of the electromagnetic actuators. The speed and displacement of the armature calculated from the coil current can be used to judge whether the armature is moving or not. Further calculating the speed of the armature's movement can provide the resultant force on the armature, and then get the retention force on the closing and on the releasing end of the armature. These can be used to verify the vibration resistance design.

V. CONCLUSION

In this paper, using the law of energy conservation, we have analyzed the source of the electromagnetic force and the armature power in an electromagnetic contactor. The example showed that the displacement and speed of the armature can be calculated using only the coil current, the mass of moving parts and the static counterforce. Since the coil current can be measured without opening the sealed shell, the ECM is non-intrusive. In particular, the movement of the armature was analyzed in detail, and the ECM between the electromagnetic power and armature speed has been established without simplifying the calculation. Using the coil current as the initial

TABLE I
FEATURES OF EXISTING METHODS

| Item | Real-time applications | Application conditions | Results | Applicable scopes |
|-------------------|------------------------|--|--|---|
| Sensors | Yes | Objects are large enough to install sensors and intrusive. | The speed and displacement of the armature, the speed and displacement of the contacts. | The fault diagnosis of the large-size electromagnetic actuators. |
| FEM | No | The dimensions, the static counterforce and the magnetic properties of the material. | The speed and displacement of the armature, the contact displacement and the speed, the coil current, the transient electromagnetic force, the transient counterforce and the contact pressure, etc. | The design and optimization of the electromagnetic actuators. |
| Simplified Models | Yes | The coil current, the coil turns, the magnetic circuit cross-section, the coefficients obtained by experimental fitting. And the armature speed need be ignored. | The displacement of the armature. | The armature control of the electromagnetic actuators. |
| SMO | Yes | The coil current and the driving voltage. Pay attention to their stability. | The speed and displacement of the armature, the resultant force. | The armature control of the electromagnetic actuators. |
| ECM | Yes | The coil current, the moving part mass and the static counterforce. | The speed and displacement of the armature, the transient electromagnetic force, the transient counterforce. | Fault diagnosis, design verification and the armature control of the electromagnetic actuators. |

point for calculation, the ECM overcomes the calculation of electromagnetic force through the magnetic circuit, thereby, reducing the complexity of calculation.

Furthermore, the ECM considers that the speed and displacement of the armature during the movement changes the magnetoresistance in the electromagnetic system, that is, the inductance of the coil changes. This means that the change in the armature during the movement is reflected through the change in coil current, regardless of whether the current is a DC or an AC. A future work may be using the ECM for calculating the dynamic welding force when the contacts arc occurs during the release process of a medium voltage circuit breaker, which is difficult to realize online testing by existing means.

It should be noted that the ECM is sensitive to the data fluctuations, and therefore requires accurate sampling of the coil current. There are 17515 time steps, and each time interval is 1e-6 seconds in the verification example. An FPGA could meet the real-time requirement.

ECM can be used for direct acting electromagnetic actuators such as relay, contactor and solenoid valve. In the case of non-direct acting actuators, the model needs to be modified according to the way of torque transmission.

REFERENCES

- [1] A. G. Espinosa, J. R. Ruiz, J. Cusido and X. A. Morera, "Sensorless control and fault diagnosis of electromechanical contactors," *IEEE Trans. Ind. Electron.*, vol. 55, no. 10, pp. 3742-3750, Oct. 2008.
- [2] P. M. d. S. D. de Moraes and A. J. Perin, "An electronic control unit for reducing contact bounce in electromagnetic contactors," *IEEE Trans. Ind. Electron.*, vol. 55, no. 2, pp. 861-870, Feb. 2008.
- [3] S. Wan and L. Chen, "Fault diagnosis of high-voltage circuit breakers using mechanism action time and hybrid classifier," *IEEE Access*, vol. 7, pp. 85146-85157, 2019.
- [4] S. Zhao and E. Wang, "Fault diagnosis of circuit breaker energy storage mechanism based on current-vibration entropy weight characteristic and grey wolf optimization support vector machine," *IEEE Access*, vol. 7, pp. 86798-86809, 2019.
- [5] S. S. Biswas, A. K. Srivastava and D. Whitehead, "A real-time data-driven algorithm for health diagnosis and prognosis of a circuit breaker trip assembly," *IEEE Trans. Ind. Electron.*, vol. 62, no. 6, pp. 3822-3831, June 2015.
- [6] Y. Kawase, O. Miyatani, T. Yamaguchi and S. Ito, "Numerical analysis of dynamic characteristics of electromagnets using 3-D finite element method with edge elements," *IEEE Trans. Magn.*, vol. 30, no. 5, pp. 3248-3251, Sept. 1994.
- [7] Y. Liu, G. Zhang, H. Qin, Y. Geng, J. Wang, J. Yang and K. Zhao, "Prediction of the dynamic contact resistance of circuit breaker based on the kernel partial least squares," *IET Gener. Transm. Distrib.*, vol. 12, no. 8, pp. 1815-1821, 2018.
- [8] Y. Hou, T. Liu, X. Lun, J. Lan and Y. Cui, "Research on monitoring system of circuit breakers based on neural networks," in *MVHI 2020*, Kaifeng, pp. 436-439, 2010.
- [9] L. Dou and S. Wang, "Characteristic parameter change of circuit breaker under closing spring fatigue," *Trans. Can. Soc. Mech. Eng.*, 2019.
- [10] Z. Zhu, Z. Yuan, L. Chen, J. He and Z. Zhu, "Vibration characteristics of thomson coil actuator based on simulation and experiments," *IEEE Trans. Energy Convers.*, vol. 35, no. 3, pp. 1228-1237, Sept. 2020.
- [11] X. Pei, A. C. Smith, R. Shuttleworth, D. S. Vilchis-Rodriguez and M. Barnes, "Fast operating moving coil actuator for a vacuum interrupter," *IEEE Trans. Energy Convers.*, vol. 32, no. 3, pp. 931-940, Sept. 2017.
- [12] C. Lee, B. H. Shin and Y. Bang, "Designing a permanent-magnetic actuator for vacuum circuit breakers using the taguchi method and dynamic characteristic analysis," *IEEE Trans. Ind. Electron.*, vol. 63, no. 3, pp. 1655-1664, Mar. 2016.
- [13] H. Zhang, B. Kou and Y. Xie, "Design and analysis of a novel modular electromagnetic actuator for micro-nano satellite application," *IEEE Trans. Energy Convers.*, vol. 36, no. 1, pp. 402-411, March 2021.
- [14] F. N. Rudsari, A. A. Razi-Kazemi and M. A. Shoorehdeli, "Fault analysis of high-voltage circuit breakers based on coil current and contact travel waveforms through modified SVM classifier," *IEEE Trans. Power Del.*, vol. 34, no. 4, pp. 1608-1618, Aug. 2019.
- [15] G. Loussert and J. D. Alzingre, "A magnetic and mechanical force model for the design of an archimedean spiral flexure bearing for a linear direct-drive electromagnetic actuator," *IEEE/ASME Trans. Mechatronics*, vol. 24, no. 4, pp. 1617-1627, Aug. 2019.
- [16] L. Shu, L. Wu, G. Wu and Z. Wu, "A fully coupled framework of predicting the dynamic characteristics of permanent magnet contactor," *IEEE Trans. Magn.*, vol. 52, no. 8, pp. 1-7, Aug. 2016.
- [17] S. Jeong, S. Lim and S. Min, "Level-set-based topology optimization using remeshing techniques for magnetic actuator design," *IEEE Trans. Magn.*, vol. 52, no. 3, pp. 1-4, March 2016.
- [18] W. Yang, J. Guo, Y. Liu and G. Zhai, "Multi-objective optimization of contactor's characteristics based on RBF neural networks and hybrid method," *IEEE Trans. Magn.*, vol. 55, no. 6, pp. 1-4, June 2019.

[19] Z. Wang, B. Lei, L. Xu, Q. Yu, W. Wen and B. Li, "Novel simulation model for coil-coil type electromagnetic repulsion actuator in low voltage DC circuit breaker," in *ISPEC 2019*, Beijing, China, pp. 1817-1821, 2019.

[20] X. Zhao, L. Li, J. Song, C. Li and X. Gao, "Linear control of switching valve in vehicle hydraulic control unit based on sensorless solenoid position estimation," *IEEE Trans. Ind. Electron.*, vol. 63, no. 7, pp. 4073-4085, July 2016.

[21] T. Braun, J. Reuter and J. Rudolph, "Observer design for self-sensing of solenoid actuators with application to soft landing," *IEEE Trans. Control Syst. Technol.*, vol. 27, no. 4, pp. 1720-1727, July 2019.

[22] T. Braun, J. Reuter and J. Rudolph, "A singular perturbation approach to nonlinear observer design with an application to electromagnetic actuators," *Int. J. Control*, vol. 93, no. 9, pp. 2015-2028, Sept. 2020.

[23] M. F. Rahman, N. C. Cheung and K. W. Lim, "Position estimation in solenoid actuators," *IEEE Trans. Ind. Appl.*, vol. 32, no. 3, pp. 552-559, May-June 1996.

[24] L. Petit, C. Prella, E. Dore, F. Lamarque and M. Biggerelle, "A four-discrete-position electromagnetic actuator: modeling and experimentation," *IEEE/ASME Trans. Mechatronics*, vol. 15, no. 1, pp. 88-96, Feb. 2010.

[25] H. Nabae and T. Higuchi, "A novel electromagnetic actuator based on displacement amplification mechanism," *IEEE/ASME Trans. Mechatronics*, vol. 20, no. 4, pp. 1607-1615, Aug. 2015.

[26] E. Ramirez-Laboreo, C. Sagues and S. Llorente, "A new model of electromechanical relays for predicting the motion and electromagnetic dynamics," *IEEE Trans. Ind. Appl.*, vol. 52, no. 3, pp. 2545-2553, May-June 2016.

[27] E. Ramirez-Laboreo and C. Sagues, "Reluctance actuator characterization via FEM simulations and experimental tests," *Mechatronics*, vol. 56, pp. 58-66, Dec. 2018.

[28] E. Ramirez-Laboreo, E. Moya-Lasheras and C. Sagues, "Real-time electromagnetic estimation for reluctance actuators," *IEEE Trans. Ind. Electron.*, vol. 66, no. 3, pp. 1952-1961, March 2019.

[29] E. Ramirez-Laboreo, M. G. L. Roes and C. Sagues, "Hybrid dynamical model for reluctance actuators including saturation, hysteresis, and eddy currents," *IEEE/ASME Trans. Mechatronics*, vol. 24, no. 3, pp. 1396-1406, June 2019.

[30] X. Wang, H. Lin, S. L. Ho, S. Fang and P. Jin, "Analysis of dynamic characteristics of permanent magnet contactor with sensorless displacement profile control," *IEEE Trans. Magn.*, vol. 46, no. 6, pp. 1633-1636, June 2010.



Jiixin You (M'14) received his Ph. D. degree in Electrical Engineering from Harbin Institute of Technology, Harbin, China, in 2014. He is currently an A. Prof. in department of electrical engineering at Harbin Institute of Technology, Harbin, China. From 2017 to 2018, he was an academic visitor with the EPE Team, ECS, University of Southampton, UK. His research interest includes the reliability of actuators with permanent magnet, modeling and simulation method for electrical apparatus and Kriging method. Mr. You is now an IEC TC94 Expert and a

Member of IEEE.



Rao Fu After receiving master's degree from Harbin Institute of technology in 2017, he had been engaged in converter research and development for one year in Delta Electronics Incorporated, Shanghai, China. Currently, he is working towards the PhD degree with the school of Electrical Engineering and Automation, Harbin Institute of Technology.

His research interests include reliability evaluation and optimal design of electrical apparatus.



Huimin Liang (M'04) received the D.S. degree in electrical engineering from Harbin Institute of Technology, Harbin, China, in 1999. She is currently a Professor in department of electrical engineering at Harbin Institute of Technology, Harbin, China.

Her research interest includes the optimization method for electromagnetic actuator with permanent magnet, modeling method for permanent magnet.



Dazhi Yang received the B.Eng., M.Sc., and Ph.D. degrees from the Department of Electrical Engineering, National University of Singapore, Singapore, in 2009, 2012, and 2015, respectively. He is currently a Professor with the School of Electrical Engineering and Automation, Harbin Institute of Technology, Harbin, China. He is the Subject Editor of Solar Resources and Forecasting, Meteorology, Grid Integration, one of the four areas of the Solar Energy Journal. He is a member of the International Energy Agency, Task 16, Solar Resource for High

Penetration and Large Scale Applications. His research interests include atmospheric radiation, solar energy meteorology, remote sensing, and spatio-temporal statistics.



Yigang Lin received his Ph.D. in Electrical Engineering from Harbin Institute of Technology in 2020. He is currently a lecturer of College of Electrical and Electronic Engineering at Wenzhou University. He researches on the reliability and testing techniques of Electrical products.



Venkata Dinavahi (Fellow, IEEE) received the B.Eng. degree in electrical engineering from the Visveswaraya National Institute of Technology, Nagpur, India, in 1993, the M.Tech. degree in electrical engineering from the Indian Institute of Technology (IIT) Kanpur, India, in 1996, and the Ph.D. degree in electrical and computer engineering from the University of Toronto, Ontario, Canada, in 2000. Presently, he is a Professor with the Department of Electrical and Computer Engineering, University of Alberta, Edmonton, AB, Canada. His research

interests include real-time simulation of power systems and power electronic systems, electromagnetic transients, devicelevel modeling, large-scale systems, and parallel and distributed computing.